Trans Indian Inst Met (December 2012) 65(6):647–651
DOI 10.1007/s12666-012-0213-y

TECHNICAL PAPER

TP 2605

Nanocomposites of Aluminum Alloys by Rapid Solidification Processing

S. S. Nayak · D. H. Kim · S. K. Pabi · B. S. Murty

Received: 15 July 2012 / Accepted: 13 September 2012 / Published online: 10 October 2012

Abstract Aluminium alloys reinforced with transition metal aluminide (Al_3Ti, Al_3Fe, Al_3Ni, etc.) particles possess high specific strength both at ambient and elevated temperature. The improved strength of these alloys are the results of slower coarsening rate of the intermetallic particles due to low diffusivity of the transition metals in aluminium. However, the strength can be enhanced further by refining the microstructure of the alloys to nanometer range. The authors have successfully attempted two important non-equilibrium processing techniques i.e. rapid solidification processing (RSP) and mechanical alloying for the refinement of the microstructure in various aluminium alloys. In this report, authors present a short review of their work on RSP of Al–Ti and Al–Fe alloys to produce nanocomposites.

Keywords Rapid solidification processing · Microstructure · Transmission electron microscopy · Hardness

S. S. Nayak (✉) · S. K. Pabi
Department of Metallurgical and Materials Engineering, Indian Institute of Technology Kharagpur, Kharagpur 721302, West Bengal, India
e-mail: sashank@uwaterloo.ca

D. H. Kim
Center for Noncrystalline Materials, Department of Materials Science and Engineering, Yonsei University, Seoul 120-749, South Korea

B. S. Murty
Department of Metallurgical and Materials Engineering, Indian Institute of Technology Madras, Chennai 600036, India

Present Address:
S. S. Nayak
Centre for Advanced Materials Joining, University of Waterloo, Waterloo, ON N2L 3G1, Canada

1 Introduction

The room temperature and elevated temperature strength of aluminium (Al) alloys is improved by adding transition metals (TM), such as Ti, Fe, Ni, Zr, Hf etc., those form intermetallic phases with Al [1–4]. In comparison to most other Al-rich intermetallic phases, Al_3TM type intermetallics are very attractive because of their lower density i.e. 75 % of the density is contributed by Al (2.7 g/cm^3). Furthermore, most of the TM has low diffusivity and solubility in aluminum [5]; hence, all the intermetallic can be expected to exhibit low coarsening rate at elevated temperature. The tetragonal DO_{22} structure of Al_3Ti intermetallic makes it brittle at room temperature which limits its industrial applications [6]. Researchers have reported two approaches to improve the ductility of Al_3Ti; micro alloying of DO_{22} structure but with little success and secondly, transforming the DO_{22} structure to the $L1_2$ (ordered cubic) [7–9]. Single phase $L1_2$–Al_3Ti intermetallics prepared by conventional casting route did not yield high ductility [9]. Thus, grain refinement was suggested to be an effective method for improving the ductility of intermetallics along with its strength [8, 10]. Metastable phases have also been reported earlier in the Al–Fe alloys prepared by RSP [11–14]. The authors have successfully attempted to develop nanocomposites of Al–Fe alloys containing 2.5–20 %Fe with refined and metastable microstructure [15].

The characterization of the different phases formed during RSP is of interest for the development of nanocomposites of Al–Ti and Al–Fe alloy systems for potential high strength applications. In this paper, a short review on the work carried out by the authors for developing nanocomposites of Al–Ti and Al–Fe alloys by RSP is reported.

2 Materials and Methods

Ingots of the master alloy with nominal compositions[1] of Al-5, 10, 15 and 20Ti and Al-2.5, 5, 10, 15 and 20Fe were prepared by either induction (Al–Ti alloys) or arc melting (Al–Fe alloys) appropriate amounts of high purity (>99.95 %) elements under argon atmosphere. For RSP experiments, pieces of the master alloy ingots were inductively re-melted in a fused silica tube and quenched onto a rotating copper wheel with linear speed in the range of 20–40 m/s. The melt spun ribbons obtained were approximately 1–4 mm in width and 15–50 μm in thickness. Phase analysis of rapidly solidified ribbons was done by X-ray diffraction (XRD) in a Rigaku CN2301 diffractometer using Cu-K_α radiation. Microstructure of rapidly solidified alloys was examined in JEOL JEM 2000EX microscope. HRTEM studies were done using a JEOL 4010 electron microscope. For electron transparency, ribbons were thinned by conventional ion milling technique. Microhardness measurements were carried out using a Vickers diamond indenter at a load of 50 g with a dwelling time of 10–15 s. At least 10–15 measurements were taken on each sample to ensure the reproducibility of the hardness values. Nanoindentation study was carried in a MTS Nano Indenter® XP using a diamond Berkovich indenter. For both micro and nanohardness measurement, ribbons were cold mounted on Bakelite followed by careful grinding using fine 1,200 grit paper to avoid the excessive removal of the specimen.

3 Results and Discussion

3.1 Nanocomposite of Al–Ti-Alloys

The XRD phase analysis of Al–Ti alloys rapidly solidified at a linear wheel speed of 40 m/s indicated that higher cooling rate has resulted in complete suppression of equilibrium tetragonal DO_{22} structure of Al_3Ti phase to form a mixture of α-Al and $L1_2$–Al_3Ti intermetallic in alloys up to 15 %Ti. An increase in the volume fraction of $L1_2$ phase with Ti content in the alloy was also observed (Fig. 1a). In contrary to lower Ti containing alloys (up to 15 %), the Al-20Ti alloy formed a large volume fraction of equilibrium DO_{22} structure of Al_3Ti along with little fraction of α-Al (Fig. 1a). An increase in volume fraction of $L1_2$–Al_3Ti phase from 24 to 42 % was measured when the Ti content of the alloy is increased from 5 to 15 % [10]; whereas a high volume fraction (78 %) of equilibrium DO_{22} phase was measured in the Al-20Ti alloy. The crystallite size measured from the XRD profiles indicated that the α-Al was in the range of 20–30 nm and $L1_2$–Al_3Ti phase was found to be in the range 20–25 nm confirming the formation of nanocomposites of Al–Ti alloys by RSP [10, 16]. The typical microstructure of the nanocomposite formed in rapidly solidified Al-15Ti alloys can be seen in Fig. 1b. Formation of a two phase mixture containing $L1_2$–Al_3Ti intermetallic particles embedded in α-Al matrix was observed. The $L1_2$–Al_3Ti particles formed in the Al-15Ti alloy was found to be in the size range 0.4–0.5 μm (Fig. 1b); however, finer particles were also observed in other alloys [10]. The selected area diffraction patterns (inset of Fig. 1b) taken from the dark particles confirmed the $L1_2$ structure of Al_3Ti phase. It is to be noted that there was no indication of any other phase formation in the nanocomposites of Al–Ti alloys apart from α-Al and $L1_2$–Al_3Ti phases. The $L1_2$–Al_3Ti phase nucleates in the melt prior to the nucleation of α-Al and during further solidification they are trapped by the fast moving solid–liquid interface of α-Al phase [17]. Further the fine-scale distribution of the $L1_2$–Al_3Ti implied that their formation involves high rate of nucleation and slow rate of growth during rapid solidification.

It is well established that hardness gives an indication of the possible strength of the any materials. The variation of Vickers hardness of the nanocomposites formed in rapidly solidified Al–Ti alloys indicated an increase in hardness with increase in Ti-content in the alloy as a consequence of increased volume fraction of $L1_2$–Al_3Ti in the nanocomposites [10, 16]. The effect of volume fraction of $L1_2$–Al_3Ti on the hardness follows a linear relationship (Fig. 2a) with a very high regression coefficient ($R^2 = 0.996$). Nanoindentation study suggested that hardness usually high at the surface (up to 400 nm) of the nanocomposites and decreases towards the interior. Similar to the Vickers hardness measurement (Fig. 2a), nanoindentation also gives high hardness value of 1.72 and 3.75 GPa ($\sim$ 168 and 367 VHN) for the Al-5Ti and Al-15Ti alloys, respectively (Fig. 2b). This confirms the high hardness of the Al–$(L1_2)Al_3Ti$ nanocomposites of binary Al–Ti alloys prepared by RSP. The high hardness of the nanocomposites was attributed to three main factors mainly (i) strengthening due to formation of $L1_2$–Al_3Ti intermetallic, (ii) solute solution strengthening due to high solute content (1.4–2.8 % Ti) in a-Al matrix, and (iii) grain size refinement of both α-Al matrix and embedded intermetallic particles in the nanometer range [10, 16]. It may be noted that the hardness of Al-20Ti alloys could not be measured due to high brittleness because of formation of DO_{22} structure phase in it.

3.2 Rapidly solidified Al–Fe Alloys

RSP of Al-alloys containing 2.5–20Fe formed supersaturated solid solution containing 0.6–1.67Fe along with the metastable phases like nanoquasicrystalline (NQ) and

[1] All compositions are in atomic percent, unless mentioned.

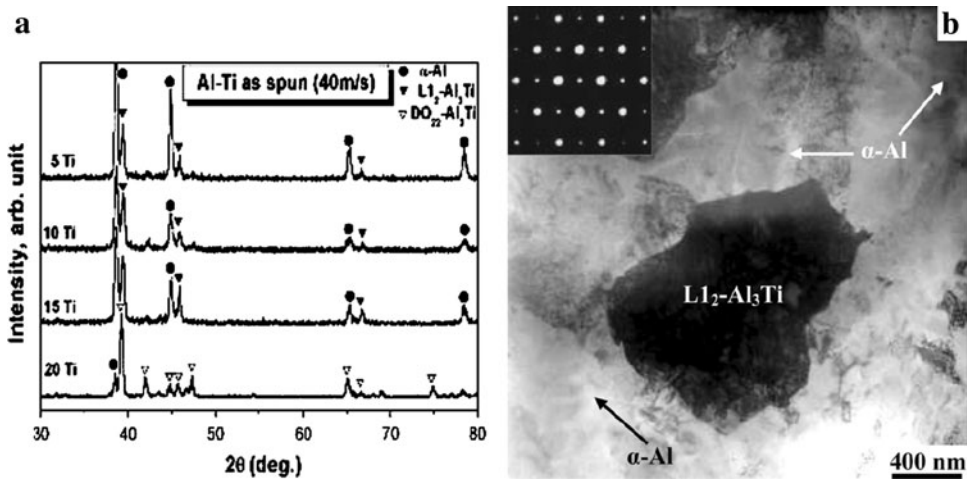

Fig. 1 **a** XRD analysis of the rapidly solidified Al–Ti alloys, **b** bright field image illustrating dendritic Al matrix (*marked*) embedded with metastable $L1_2$–Al_3Ti particles (*dark*) in rapidly solidified Al–15Ti alloy [10]

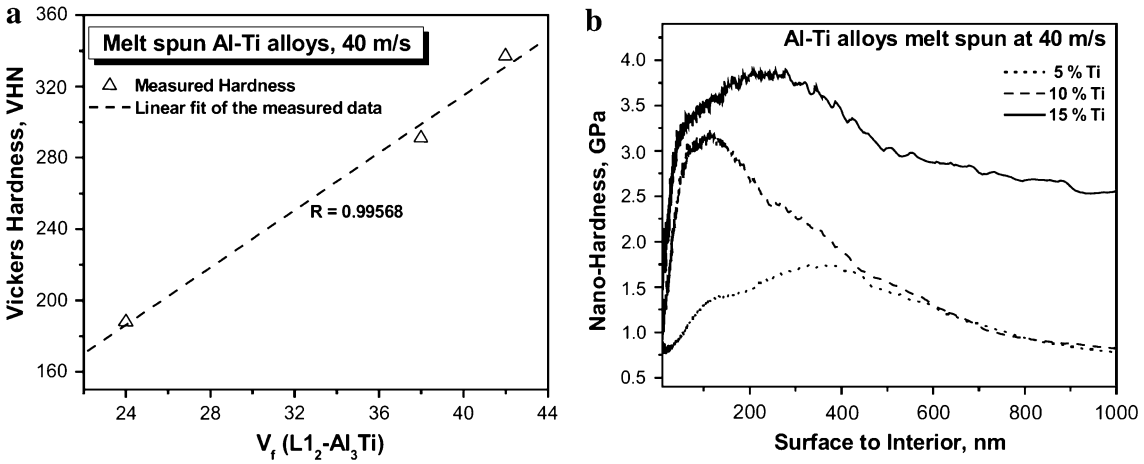

Fig. 2 Hardness of Al–Ti alloys melt spun at 40 m/s wheel velocity: **a** Vickers hardness as a function of volume fraction of $L1_2$–Al_3Ti; **b** variation of nano-hardness with depth from the surface of the specimen [10, 16]

amorphous phase; NQ phases were reported for the first time in the Al–TM alloys containing solute (Fe) as low as 2.5 and 5 % [14–16]. Due to the ultra-fine size of the particulates dispersed in the melt spun alloys, their nature could not be identified easily through the conventional SAED patterns. Hence, HRTEM was employed to ascertain the presence of NQ in the melt spun Al–Fe alloys. Figure 3 shows the HRTEM images of Al–5Fe alloy melt spun at 40 m/s. The HRTEM image (Fig. 3a) reveals the NQ phase distribution (dark particles) in the nano-cellular region in thickness range 10–15 nm (marked by arrows) and relatively coarse cells of α-Al (80–100 nm). The energy dispersive X-ray microanalysis in HRTEM showed that the intercellular regions were rich (31.6 %) in Fe content and cells have low (2.0 %) Fe content [15]. The composition of intercellular region was found to be slightly higher than the common quasicrystalline composition, which is close to Al_3Fe or $Al_{13}Fe_4$. This could be attributed to the presence of Fe-rich NQ and amorphous phases being the last solidification products in the intercellular regions. During the non-equilibrium solidification process in RSP, the high undercooling of melt resulted in the crystallization of fine grained α-Al. With the progress of solidification front, the remaining liquid in the intercellular regions get enriched in Fe and solidified last leading to the metastable phase formation, viz. NQ and/or amorphous phase [14–16]. Figure 3b displays another HRTEM image of Al–5Fe alloy melt spun at 40 m/s. The Fast Fourier transformation–selected area diffraction pattern from the dark nanocrystals in the square region, marked with white dotted lines, depicts the spots from 3-fold symmetry axis of the NQ phase. This confirms the presence of NQ phase in the intercellular regions separating the cells of α-Al phase, as discussed in the previous paragraph, in the melt spun Al–5Fe alloy leading to the formation of a metastable nanocomposite.

The HRTEM images of the melt spun Al–10Fe alloy melt spun at 40 m/s are illustrated in Fig. 4. A close look of

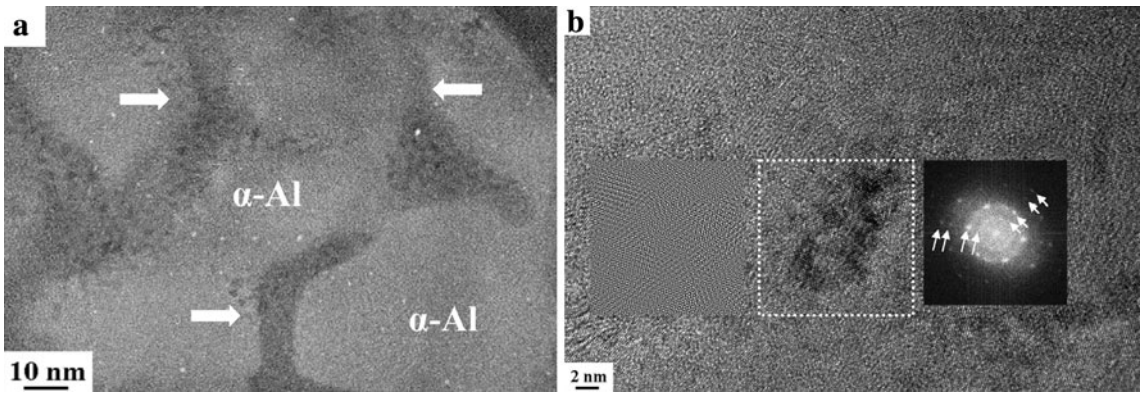

Fig. 3 HRTEM images of Al–5Fe alloy melt spun at 40 m/s: **a** low-magnification image showing nano-cellular structure with distribution of dark NQ particles, **b** high magnification image depicting NQ phase: inset FFT–SAED pattern on *right* in **b** was obtained from the *square marked region* revealing the 3-fold symmetry pattern, and the reverse FFT image is shown on *left* side [15, 16]

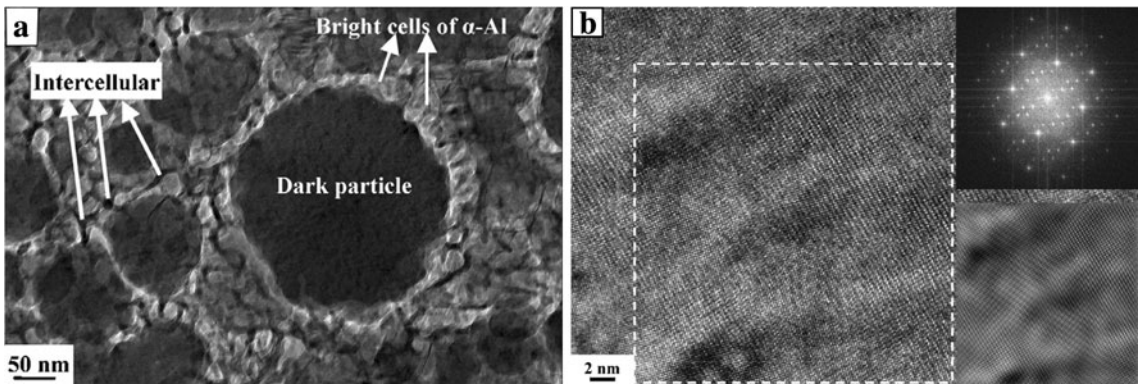

Fig. 4 HRTEM images of Al–10Fe alloy melt spun at 40 m/s: **a** showing microstructure with NQ nodules embedded in cellular matrix of α-Al with intercellular NQ regions, **b** illustrating NQ phase. 2-fold symmetry in the FFT-SAD pattern (*top-right* inset in **b**) and inverse FFT from the FFT-SAD pattern (*bottom-right* insert in **b**) are also displayed [15, 16]

the image indicated that the dark particles seen are not single grain, but contains many fine precipitates inside (Fig. 4a). The microstructure revealed that these fine dark particles are embedded in a matrix of bright cells with dark intercellular boundaries as marked by arrows in Fig. 4a. Like the Al–5Fe alloy, the matrix in Al–10Fe alloy also had microcellular structure containing bright α-Al cells (20–30 nm) separated by a few nanometer thick (10–15 nm) Fe rich dark intercellular line (Fig. 4a). However, the α-Al cells were finer (20–30 nm) compared to Al–5Fe alloy (50–60 nm) solidified with similar cooling rate (40 m/s). The quasicrystalline nature of the nano-dispersoids in the melt spun Al–10Fe alloy was further confirmed by high resolution image (Fig. 4b). The FFT image of the white dashed region yielded the diffraction pattern parallel to 2-fold symmetry axis of quasicrystalline phase. The inverse FFT image of this diffraction pattern generated a microstructure analogous to the original HRTEM image inside the white dotted region (shown as inset) confirming the area selected was NQ region in the sample (Fig. 4b). It was concluded that the NQ related phases observed are metastable phases which nucleate and grow over a wide range of compositions and cooling rates, which are slow enough to permit the atomic rearrangement in the liquid, but rapid enough to prevent crystallization of equilibrium phases from the melt [15].

Hardness values of the nanocomposites in Al–Fe alloys are plotted in Fig. 5 as a function of Fe content and linear wheel speeds. It was observed that irrespective of the composition, hardness value increases with increase in cooling rate during melt spinning, giving maximum value at wheel speed of 40 m/s. Increase in hardness of the nanocomposites formed in melt spun Al–Fe alloys at high cooling rate (wheel speed) is due to formation of metastable phases or increase in their volume fraction, if at all they form at lower cooling rates. The optimum composition for better hardness was found to be Al–10Fe which had the highest hardness amongst all the alloys studied, irrespective of the wheel speed used (Fig. 5). For Al–Fe alloys, the variation of hardness was observed to be similar to ageing

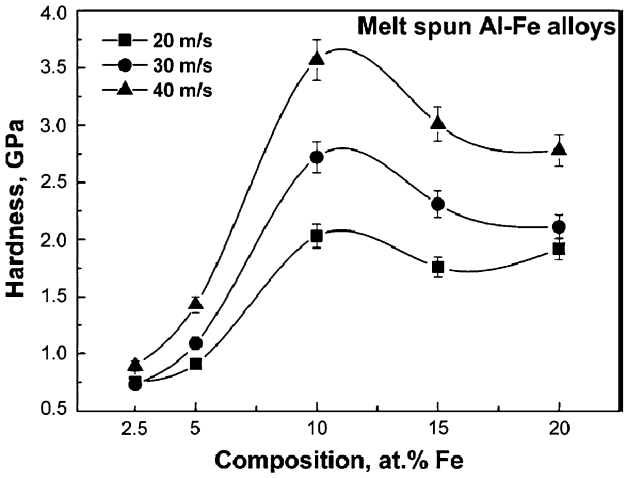

Fig. 5 Variation of microhardness as a function of Fe content in Al–Fe alloys melt spun at different wheel speeds [15, 16]

curve suggesting that the optimum value of hardness could be achieved in composition of 10 %Fe with higher cooling rate (40 m/s) amongst all the alloys studied. The peak hardness for Al–10Fe alloy is attributed to formation of higher volume fraction of NQ phase and its coexistence with amorphous phase. Also, higher solute content, 9.17 % Fe as measured by EDX [15, 16], in α-Al matrix enhances the hardness due to solid solution hardening. Furthermore, the grain size (cell size) of α-Al matrix was finer in Al–10Fe alloy compared to Al–5Fe alloy [15], which resulted in increase in its hardness further as per Hall–Petch strengthening. It was thus concluded that nanocomposites prepared by RSP give better mechanical properties for Al–10Fe alloy that has metastable microstructure of NQ phase and α-Al.

4 Summary

Al–Ti alloys: Al-based nanocomposites with nanocrystalline $L1_2$–Al_3Ti precipitates have been successfully prepared in binary Al–Ti alloys by RSP. Higher cooling rate was observed to suppress the formation of equilibrium DO_{22}–Al_3Ti phase. Hardness values of binary Al–Ti were observed to increase linearly with increase in the volume fraction of $L1_2$–Al_3Ti. High hardness of 340 VHN (∼ 3.46 GPa) was obtained in the nanocomposite containing 42 % of $L1_2$–Al_3Ti precipitates in Al-15Ti alloy. Nanoindentation studies further confirmed the high hardness of the nanocomposites.

Al–Fe alloys: Nanocomposite structure with NQ phases precipitated in Al-matrix was obtained in the Al–alloys with solute content below 5 %. Non-equilibrium solidification in RSP resulted in unique coexistence of the NQ phase and amorphous phase with α-Al. High hardness value (∼ 3.57 GPa) measured in Al–10Fe alloy melt spun at 40 m/s was attributed to solid solution strengthening by the high solute content (∼ 9.17 %Fe), dispersion strengthening by high volume fraction of NQ phase, and Hall–Petch strengthening from finer cell size (20–30 nm) of α-Al matrix. Hardness of melt spun Al–Fe alloys was observed to increase with the cooling rate i.e. increasing the linear wheel speed.

References

1. Ryum N, *Acta Metall* **17** (1969) 269.
2. Tong X C, and Fang H S, *Metall Mater Trans A* **29A** (1998) 893.
3. Wang S H, and Kao P W, *Acta Mater* **46** (1998) 2675.
4. Varin R A, *Metall Mater Trans A* **33A** (2002)193.
5. Das S K, and Davis L A, *Mater Sci Eng A* **98** (1988) 1.
6. Pandey A B, Mishra R S, and Mahajan Y R, *Acta Metall Mater* **40** (1992) 2045.
7. Yamaguchi M, and Umakoshi Y, *Prog Mater Sci* **34** (1990) 1.
8. Baker I, and Monroe P R, *J Met* **40** (1988) 28.
9. Yamaguchi M, and Inui H, in *Intermetallic Compounds*, (eds) Westbrook J H, and Fleischer R L, Wiley, New York (1994), p. 147.
10. Nayak S S, Kim D H, Pabi S K, and Murty B S, *Intermetallics* **18** (2010) 487.
11. Nasu S, Gonder U, and Preseton R S, *J Physique* **41/C1** (1980) C1-385.
12. Blank E, *Z Metallk* **63** (1972) 315.
13. Badan B, Magrini M, and Zambon A, *Scripta Mater* **35** (1996) 13.
14. Nayak S S, Murty B S, and Pabi S K, *Bull Mater Sci* **31** (2008) 449.
15. Nayak S S, Chang H J, Kim D H, Pabi S K, and Murty B S, *Mater Sci Eng A* **528** (2011) 5967.
16. Nayak Sashank Nayak, *Synthesis and Characterization of Nanocrystalline Intermetallics and Nanocomposites in Al-TM (TM = Ti, Zr, Fe) Alloys Prepared by Non-equilibrium Processing Routes,* PhD Thesis, Indian Institute of Technology, Kharagpur (2007).
17. Cotton J D, and Kaufman M J, *Metall Mater Trans A* **22** (1991) 927.